Supporting information

Double exchange interaction promoted high-valence metal sites for neutral oxygen evolution reaction

Jisi Li, Jingjing Ma, Kun Du, Erling Zhao, Jiaxin Guo*, Jing Mao*, Tao Ling*

Contents

Experimental details

Synthesis of pristine and heteroatom-doped CoO nanorods on carbon fiber substrate. CoO nanorods were directly synthesized on carbon fiber substrate by a cation exchange method using ZnO NRs as structural templates described in our previous work.[1-4] Specially, doping precursor (VCl_3 or $MnCl_2$ or $NiCl_2$) and cobalt chloride ($CoCl_2$) powder were placed 2.5 cm upstream from the tube center to synthesize heteroatom-doped CoO nanorods (Fig. S1). For the synthesis of pristine CoO nanorods, pure $CoCl_2$ was used. The loading mass of as-synthesized pristine and heteroatom-doped CoO nanorods was ~0.2 mg cm^{-2}.[5]

Synthesis of V, Mn and Ni oxide nanorods on carbon fiber substrate. Pure V, Mn and Ni oxide nanorods were prepared by cation exchange method, similar as pristine CoO nanorods. Specifically, VCl_3 or $MnCl_2$ or $NiCl_2$) powder was placed 2.5 cm upstream from the tube center. The exchange temperature for V oxide was 550 ^oC and for Mn and Ni oxides was 600 ^oC.

Materials characterization. Scanning electron microscopy (SEM) and transmission electron microscopy (TEM) were characterized on a Hitachi S-4800 SEM and a JOEL 2100 TEM, respectively. X-ray diffraction (XRD) was performed on a Bruker D8 advance X-ray diffractometer. X-ray Photoelectron Spectroscopy (XPS) was carried out on a kalpha Thermo Fisher spectrometer (Thermo Fisher Scientific). The base pressure was about 3×10^{-9} mbar and the binding energies were referenced to the C 1s line at 284.8 eV from adventitious carbon. Electron paramagnetic resonance (EPR) was characterized on a JES-FA200 Electron spin paramagnetic resonance spectrometer, at liquid nitrogen temperature (-70 K) and applied potential of 1.6 V versus reversible hydrogen electrode (RHE).

Electrochemical characterization. Electrochemical measurements were performed in a three-electrode electrochemical cell using a calomel electrode saturated in KCl solution as the reference electrode, a graphite rod as the counter electrode and a electrocatalyst-loaded carbon fiber paper as the working electrode. The electrode potential was calibrated with respect to RHE in the high purity hydrogen saturated electrolyte and Pt worked as the working electrode. The polarization curves were recorded in 1 M phosphate buffer saline (PBS, pH=7) with a scan rate of 5 mV s^{-1}.

Supplementary Figures

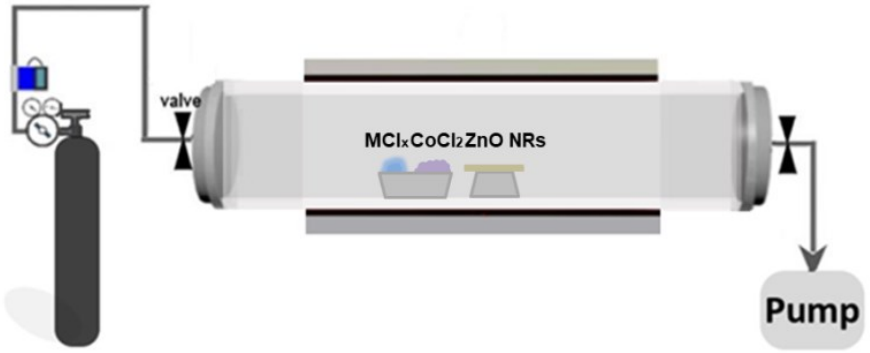

Figure S1. Synthetic schematic diagram of heteroatom-doped CoO nanorods. For the cation exchange process, the furnace was heated to 600 ^{o}C and maintained for 30 min under nitrogen gas flow (50 s.c.c.m.), then cooled to room temperature.

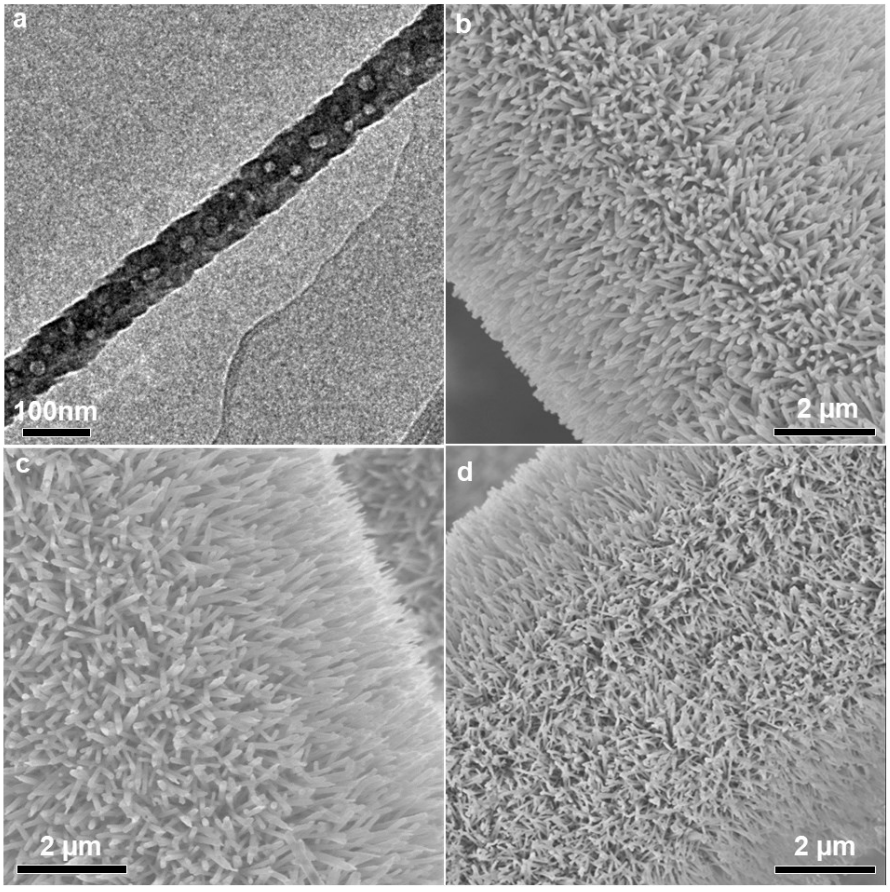

Figure S2. Characterization of pristine and heteroatom-doped CoO nanorods. (a) TEM of a single V-doped CoO nanorod. (b)-(d) SEM images of pristine, Mn-, and Ni-doped CoO nanorod arrays on carbon fiber, respectively.

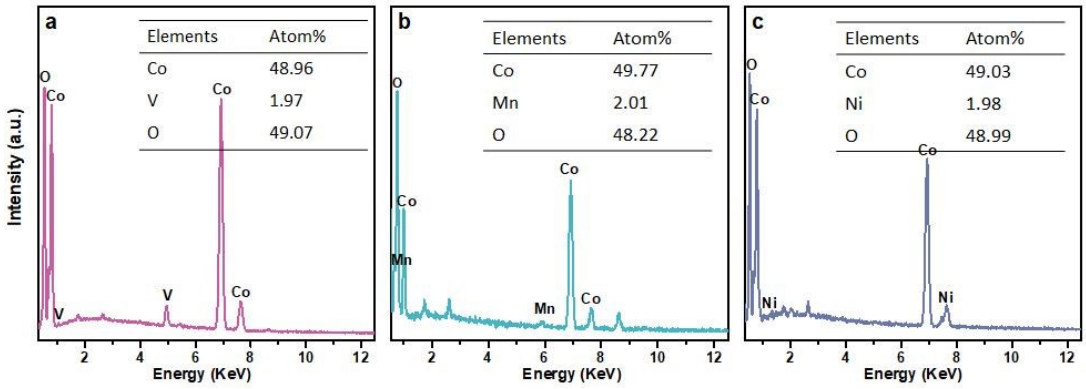

Figure S3. (a)-(c) EDS analysis of V-, Mn-, and Ni-doped CoO nanorods, respectively.

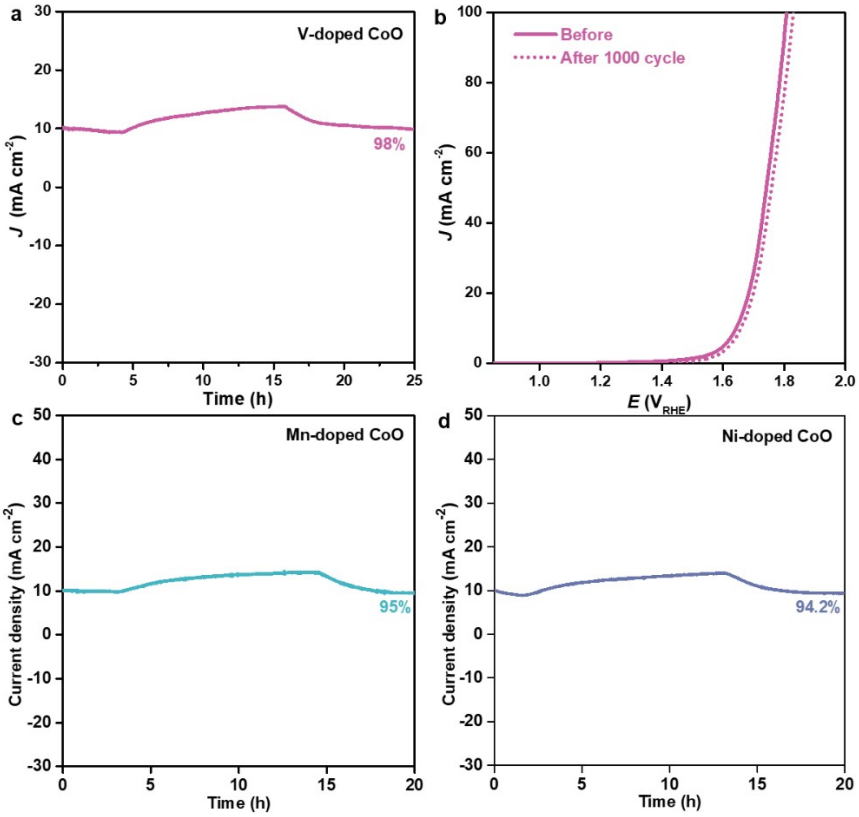

Figure S4. (a), (c) and (d) Chronoamperometric responses of V-, Mn- and Ni-doped CoO nanorods, respectively. (b) OER polarization curves of V-doped CoO nanorods before and after 1000 potential sweeps with scan rate of 100 mV s^{-1} in 1.0 M PBS (pH=7) solution.

The chronoamperometric response demonstrates the high stability of the V-doped CoO nanorods, showing only a slight current attenuation of 2% after 25 h continuous testing (a). The accelerated stability test also confirms its reliable stability with slight shift of the OER polarization after 1000 continuous potential cycles (b). Similar stability was observed in the Mn- and Ni-doped CoO nanorods (c and d).

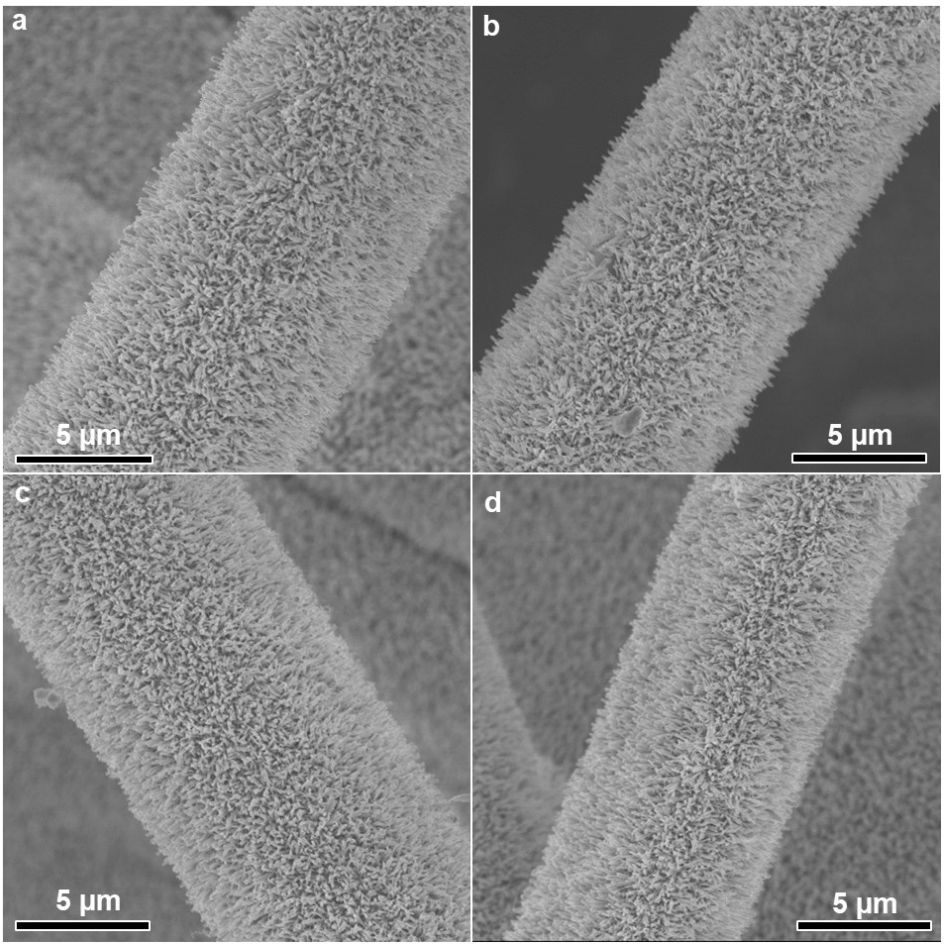

Figure S5. (a)-(d) SEM images of V-, Mn- and Ni-doped and pristine CoO nanorods after stability test, respectively, showing that the morphology of the nanorods was well preserved after the stability test.

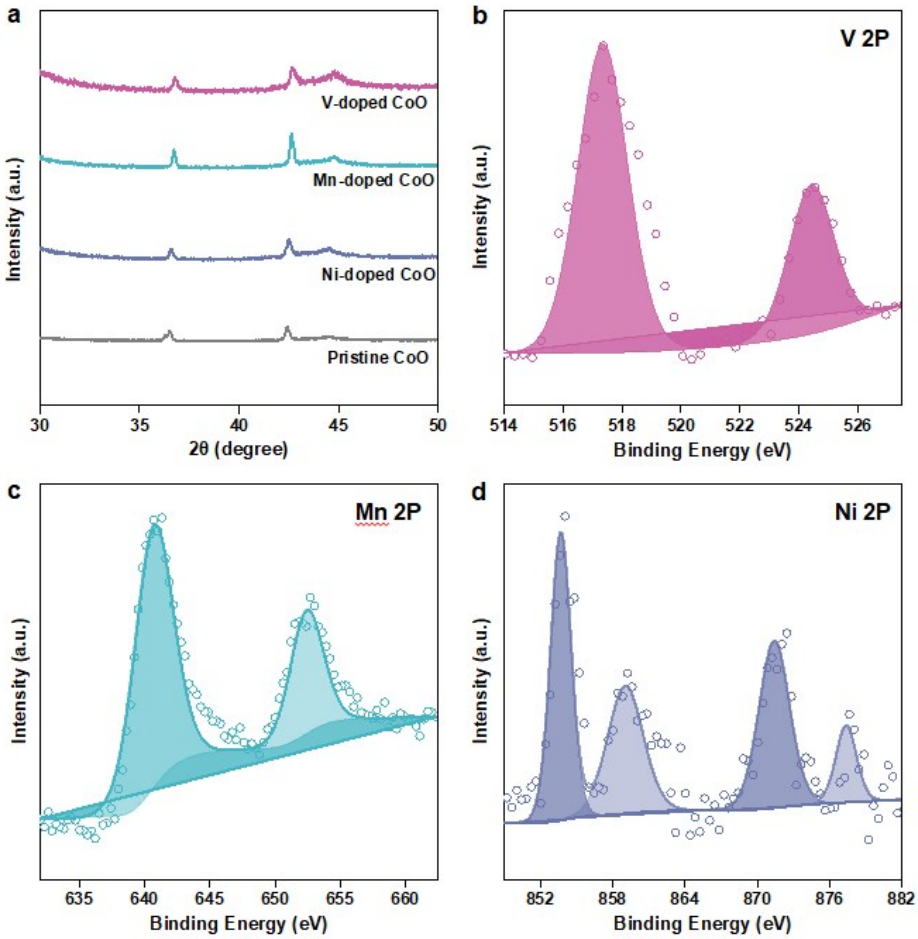

Figure S6. (a) XRD spectra of pristine and V, Mn, Ni-doped CoO nanorods. (b) V 2p, (c) Mn 2p, and (d) Ni 2p XPS spectra of heteroatom-doped CoO nanorods after stability test.

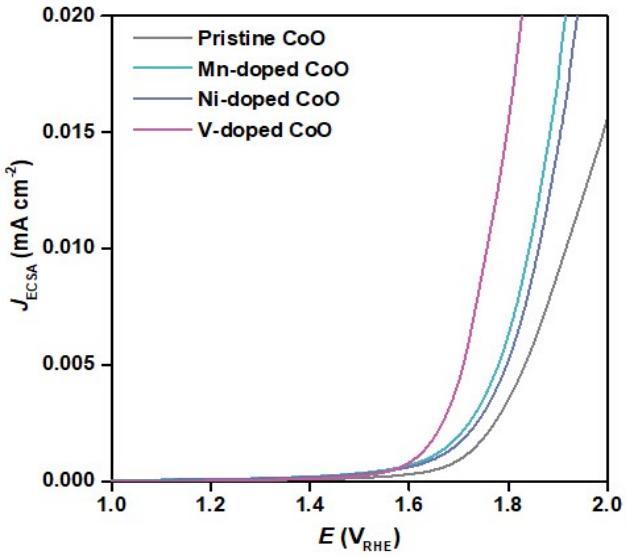

Figure S7. Electrochemically active surface areas (ECSA)-normalized LSV curves of pristine and heteroatom-doped CoO nanorods.

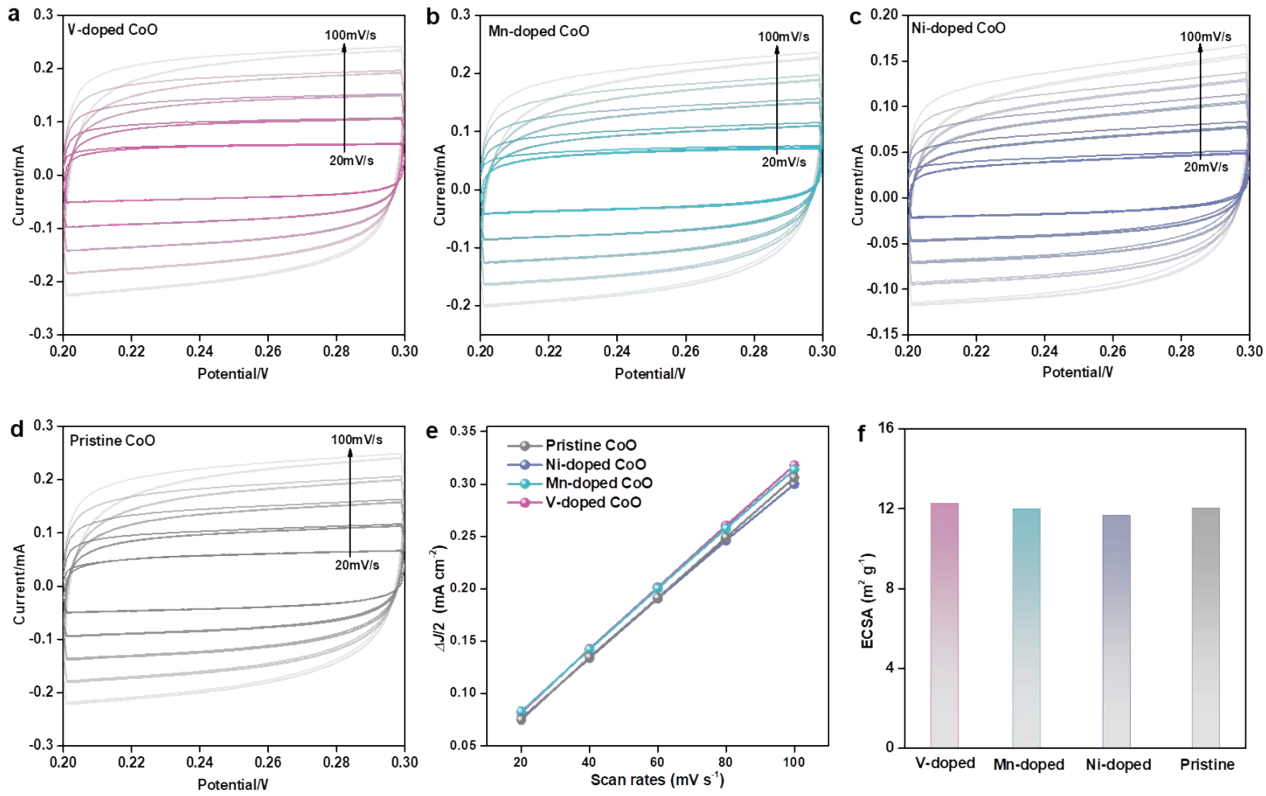

Figure S8. Estimation ECSAs of catalysts. (a)-(d) Cyclic voltammetry (CV) curves of V-, Mn-, Ni-doped and pristine CoO nanorods in 1.0 M PBS, respectively. (e) Plots of current density versus scan rate to determine the double layer capacitance (C_{dl}). (f) Calculated ECSAs of V, Mn, Ni-doped and pristine CoO.

ECSA was calculated by the equations:

$$\text{ECSA}=\frac{R_f}{m_{loading}} \qquad \text{(S1)}$$

$$R_f=\frac{C_{dl}}{C_s} \qquad \text{(S2)}$$

where R_f is the roughness factor of catalyst, C_s is the specific capacitance of 60 μF cm^{-2} for oxide, and $m_{loading}$ =0.2 mg cm^{-2} is the mass-loading of the nanorod catalysts. As shown in (f), the ECSAs for the pristine and the heteroatom-doped CoO nanorods are almost identical.

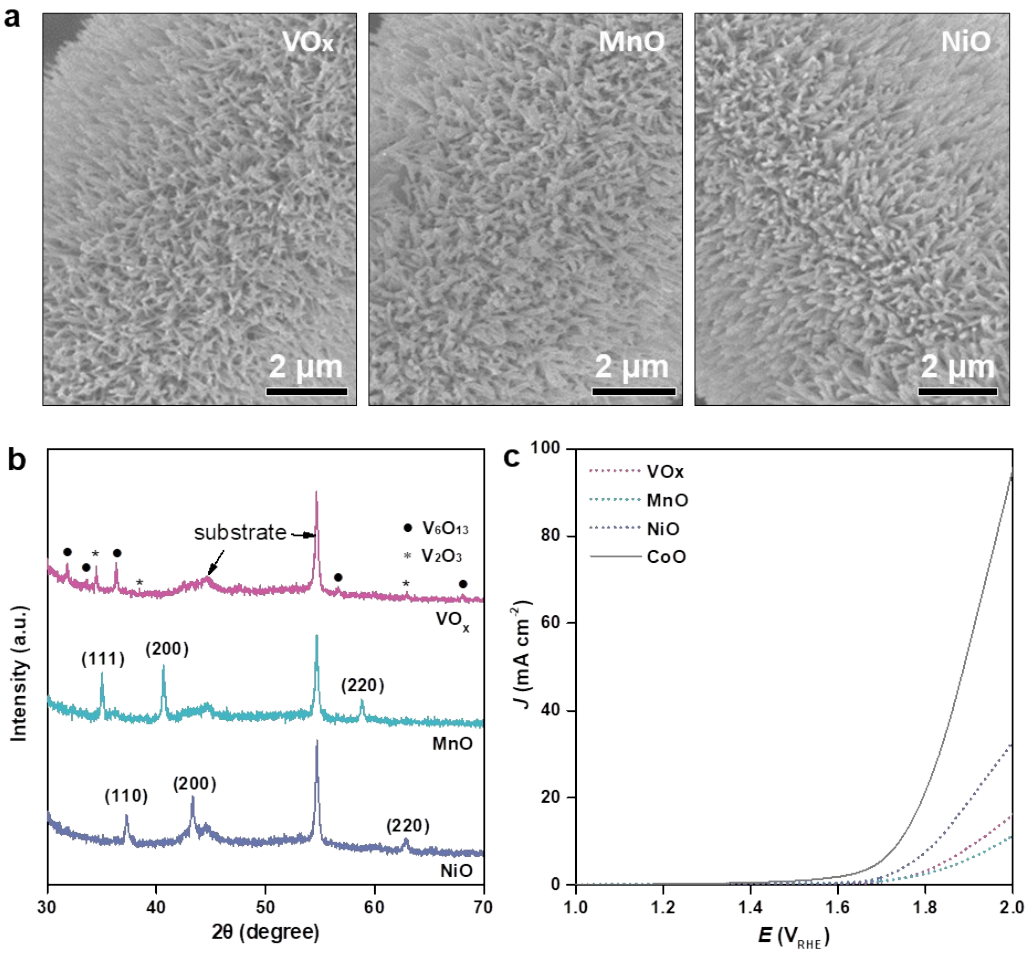

Figure S9. (a)-(c) SEM images, XRD spectra and neutral OER performance of VO_x, MnO and NiO nanorods, respectively. As shown, the performance of these oxides was far inferior to that of the pristine CoO under identical test conditions, indicating that the dopants themselves were not active sites for neutral OER.

Supplementary Figures

Table S1. Comparison of electrochemical performances of Co-contained water oxidation electrocatalysts in mild condition.

Electrocatalysts	Overpotential (mV)	Tafel slope (mV dec^{-1})	Electrolyte	Ref.
V-doped CoO	412 @ 10mA cm^{-2}	133	pH 7, 1.0 M PBS	This work
Co/ZnO	450 @ 10mA cm^{-2}	106	0.1 M PBS	[6]
Co–Pi film	410 @ 1mA cm^{-2}	--	pH 7, 0.1 M KPi	[7]
CeO_2/Co–Bi	453 @ 10mA cm^{-2}	120	pH 7.4, 0.1 M PBS	[8]
Co-DP-MP@NCF[a]	577 @ 30 mA cm^{-2}	129	0.1 M PBS	[9]
AC-$Co_2(OH)_3Cl$[b]	600 @ 47 mA cm^{-2}	155	1.0 M PBS	[10]

[a]$Co(H_2PO_4)_2/Co(PO_3)_2$ @ nanocarbon florets; [b]activation derived $Co_2(OH)_3Cl$ components

Supplementary References

1. C. Mu, J. Mao, J. Guo, Q. Guo, Z. Li, W. Qin, Z. Hu, K. Davey, T. Ling and S. Z. Qiao, *Adv. Mater.* 2020, **32**, 1907168.
2. Y.-J. Li, L. Cui, P.-F. Da, K.-W. Qiu, W.-J. Qin, W.-B. Hu, X.-W. Du, K. Davey, T. Ling and S.-Z. Qiao, *Adv. Mater.* 2018, **30**, 1804653.
3. T. Ling, P.-F. Da, X.-L. Zheng, B.-H. Ge, Z.-P. Hu, M.-Y. Wu, X.-W. Du, W.-B. Hu, M. Jaroniec and S.-Z. Qiao, *Sci. Adv.* 2018, **4**, 6261.
4. C. Meng, T. Ling, T.-Y. Ma, H. Wang, Z. Hu, Y. Zhou, J. Mao, X.-W. Du, M. Jaroniec and S.-Z. Qiao, *Adv. Mater.* 2017, **29**, 1604607.
5. T. Ling, D.-Y. Yan, Y. Jiao, H. Wang, Y. Zheng, X. Zheng, J. Mao, X.-W. Du, Z. Hu, M. Jaroniec and S.-Z. Qiao, *Nat. Commun.* 2016, **7**, 12876.
6. C. Meng, Y.-F. Gao, X.-M. Chen, Y.-X. Li, M.-C. Lin and Y. Zhou, *ACS Sustain. Chem. Eng.* 2019, **7**, 18055-18060.
7. Y. Dong, C. W. Oloman, E. L. Gyenge, J. Su and L. Chen, *Nanoscale* 2020, **12**, 9924-9934.

8. X. Zhou, S. Guo, Q. Cai and S. Huang, *Nanoscale Adv.* 2019, **1**, 3686-3692.

9. J. Saha, S. Verma, R. Ball, C. Subramaniam and R. Murugavel, *Small* 2020, **16**, 1903334.

10. H. Jiang, Q. He, X. Li, X. Su, Y. Zhang, S. Chen, S. Zhang, G. Zhang, J. Jiang, Y. Luo, P. M. Ajayan and L. Song, *Adv. Mater.* 2019, **31**, 1805127.